Photonic band structure of dielectric membranes periodically textured in two dimensions

V. Pacradouni, W. J. Mandeville, A. R. Cowan, P. Paddon, and Jeff F. Young
Department of Physics and Astronomy, University of British Columbia, Vancouver, British Columbia V6T 1Z4

S. R. Johnson
Center for Solid State Electronics Research, Arizona State University Tempe, Arizona 85287-6206

(Received 2 March 2000)

The real and imaginary photonic band structure of modes attached to two-dimensionally textured semiconductor membranes is determined experimentally and theoretically. These porous waveguides exhibit large (1000 cm^{-1} at 9500 cm^{-1}) second-order optical gaps, highly dispersive lifetimes, and bands with well-defined polarization along directions of high symmetry.

The past decade has seen much progress in understanding the fascinating properties of photonic crystals.[1,2] It is now well-established that two-dimensional (2D) and 3D dielectric texture can be used to produce artificial optical materials that exhibit full photonic bandgaps, or ranges in frequency over which it is classically impossible to propagate light in any direction, with any polarization. Furthermore, defects in the respective dielectric lattices can support photon modes that are *localized* in 2D or 3D. Such structures having lattice constants on the order of centimeters have been used in the microwave region as high-Q filters and broadband reflective antennae platforms.[3]

Semiconductor heterostructures, in many senses, make ideal hosts for photonic crystals. The refractive index difference between air and several important Group-IV and Group-III-V semiconductors, $\Delta n \sim 2.5$, is sufficient to allow the formation of complete optical bandgaps using the appropriate lattice geometries.[4] Artificial semiconductor quantum wells, wires and dots can be formed in a number of ways to achieve tunable electronic properties (resonant frequencies, densities-of-states) throughout the near infrared part of the spectrum. Thus it will soon be possible to independently tune the electronic *and* photonic properties of semiconductor heterostructures in order to realize qualitatively new quantum electronic phenomena based on the concept of photonic bandgaps.[5,6]

There are significant challenges to achieving 3D texture in crystalline semiconductors on the required length scales ($\sim 200-500$ nm). However, deep 2D texture with these dimensions is achievable, although not trivially. Given the importance of slab waveguides in present optical communications devices, 2D textured semiconductor waveguides offer a medium for exploring the effects of photonic band structure engineering in a practically useful geometry.[7–14] Recently, Painter *et al.*[15] fabricated an optically pumped infrared laser based on a photonic defect state in a 2D-textured semiconductor waveguide. This demonstrates the power and potential of these concepts in the optoelectronic context.

In this paper we quantitatively address the fundamental properties of electromagnetic modes localized in the vicinity of thin, 2D-textured semiconductor membranes. These structures represent an intriguing limit of 2D photonic crystals that are not translationally invariant in the direction perpendicular to the texture. The purpose of the present paper is to identify and quantify the effects of relaxing this translational invariance on the structure's photonic eigenstates. By successfully comparing an electromagnetic model[12] with our experimental optical scattering data, we show that these eigenstates can largely be understood as renormalized TE-polarized slab modes that contain *essential* TM-polarized field components. The renormalization caused by scattering of the slab modes from the 2D texture leads to dramatically altered dispersion (measured second-order gaps $\sim 10\%$ of the center frequency), and finite lifetimes (Q's) that exhibit wide variation over the Brillouin zone.

Figure 1 schematically shows the sample structure used to obtain the data reported below. It consists of an air/AlGaAs/Al-oxide waveguide which, in the absence of the 2D array of pores, would support only a single TE polarized bound mode in the near infrared. It was fabricated using molecular-beam epitaxy, electron-beam lithography, dry-etching, and wet-oxidation techniques.[16]

As previously discussed by us and others,[7,12,14] the energy of the leaky modes is revealed through Fano-like features in the specular reflectivity spectrum of a broadband collimated source incident on the porous waveguide at a well-defined angle. Reflectivity spectra were collected for various incident angles using a $\theta - 2\theta$ setup employing reflective optics, a polarizer, and a Fourier transform interferometer.

Figure 2(a) shows the *p*-polarized reflectivity spectrum as obtained from the experiment and from the model calculation[12,17] for the case of *p*-polarized light incident at $\theta = 5^0$ along the Γ-X symmetry direction ($\phi = 0^0$) of the

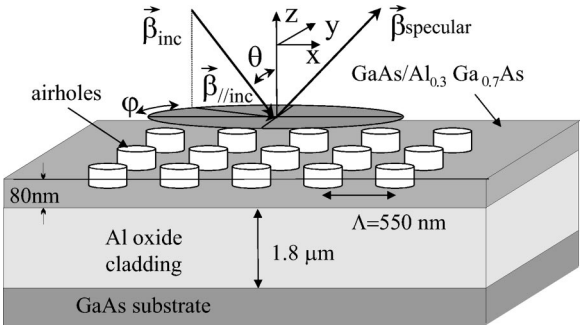

FIG. 1. Sample structure and scattering geometry.

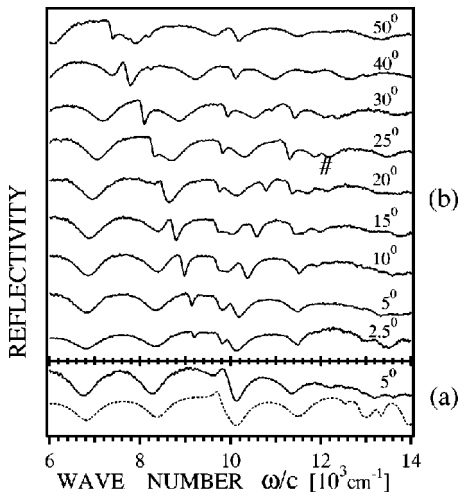

FIG. 2. Reflectivity spectra for light incident along $\Gamma - X$: (a) Experimental (solid line) and model (dotted line) reflectivity spectra for *p*-polarized radiation incident at 5^0; (b) Experimental spectra for *s*-polarized radiation incident at various angles.

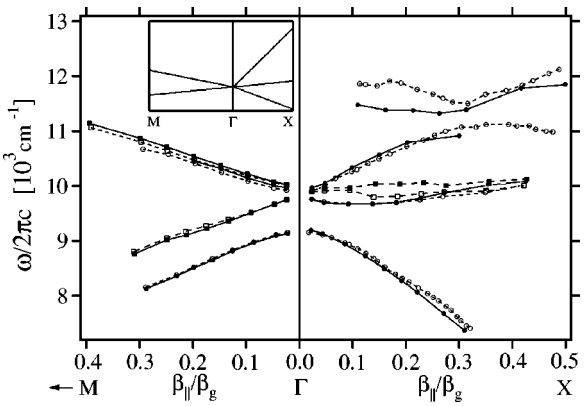

FIG. 3. Real part of band structure for the structure in Fig. 1: mode frequency versus magnitude of in-plane wave vector for experiment (solid lines and markers) and model (dotted lines and hollow markers) for *s* (circles) and *p* (squares) polarized radiation. The inset schematically depicts the band structure for the case of weak texture.

square Brillouin zone. Similar quality spectra were obtained from over 12 related structures with pitches ranging from 500 nm to 575 nm. The broad features are Fabry-Perot fringes due to the cavity formed by the 1.8 μm Al-oxide layer; they would be present in the absence of the 2D grating. The sharper bipolar feature indicates resonant coupling to a leaky slab mode attached to the textured waveguide structure. Figure 2(b) shows a scaled series of *s*-polarized reflectivity spectra taken at different angles of incidence θ with the in-plane momentum always oriented along the Γ-X direction of the Brillouin zone.

These reflectivity spectra reveal much about the nature of electromagnetic modes localized to porous membranes. The basic dispersion of various bands excited by *s*-polarized radiation can be deduced by cursory inspection. There are clear gaps, or avoided crossings at the zone center. Comparison of the *s* and *p* polarized spectra at $\theta = 5^0$ reveals the fact that modes from different bands are excited *either* by *s or* by *p* polarized radiation when probed along the Γ-X direction. The same is true for excitation along the Γ-M symmetry direction. Finally, the linewidths of the modes varies considerably from band to band, and within bands. Detailed experimental and model analysis suggests that each leaky mode in this 2D periodic waveguide geometry should be characterized by an energy, a lifetime, and a polarization label. The nontrivial variation of all these characteristics makes the corresponding photonic band structure much richer than in pure 2D or 3D photonic crystals.

The widths and positions of the obvious resonant features in these and other spectra were extracted by fitting them with Fabry-Perot and Fano lineshape functions. Figure 3 shows the resulting dispersion of the resonant modes of the structure along high-symmetry directions of the square Brillouin zone. Figure 3 also shows the dispersion as calculated[12,17] using the parameters given in Fig. 1. The significance of the dispersion lies in how it differs from that which would be obtained from a similar structure if the array of holes were only etched a small fraction of the way through the membrane. In that case the corresponding dispersion curves would effectively represent the bare TE polarized slab mode dispersion zone folded to the first Brillouin zone by the in-plane Fourier components of the square grating. The inset to Fig. 3 schematically illustrates that situation.

The effect of the strong periodic scattering in the fully-etched membrane is, therefore, to lift degeneracies and to flatten bands near ''gaps'' that open both at the center of the Brillouin zone, and at interior points where certain zone-folded bands cross. Note that the lifting of the degeneracies, with respect to the center frequencies, and the extent of the bandbending, with respect to the width of the first Brillouin zone, are on the order of 10%. This is a measure of the degree to which the photonic properties of the membrane are different from those of the bare slab. For reference, the optical gaps in the 1D textured waveguides used in commerical distributed feedback lasers are only $\sim 0.1\%$.

It is an important property of these structures that for light incident along the crystal symmetry directions ($\phi = 0^0$ and $\phi = 45^0$ in the present case) there is no *s*-*p* or *p*-*s* scattering in the specular direction. That is, the polarization of the radiative component of the eigenmodes is a ''good quantum number'' and has, therefore, been used to label the curves in Fig. 3. Notice that a given *band* cannot be given a unique polarization label because away from directions of high symmetry, leaky eigenmodes will in general radiate an elliptically polarized field. Indeed, the fourth highest energy band shown in Fig. 3 radiates *s*-polarized light along the Γ-X direction, and *p*-polarized light along the Γ-M direction.

At first it might seem unusual that eigenmodes that are all dominated by TE-polarized field components might be labeled as *p* polarized. In fact, it is the relatively small but essential zeroth-order Fourier field component (the one lying within the first Brillouin zone) that determines the polarization selection rules for these modes, since this is the only part of the Bloch state that can be phase matched to plane waves propagating above the membrane. This zeroth-order component of the polarization field associated with the Bloch states is a superposition of the dominant (first order) TE-polarized field components as they scatter via the first-order Fourier components of the dielectric texture. The resulting polarization can therefore only be *s* or *p* along lines of the Brillouin zone that possess mirror symmetry, since the cor-

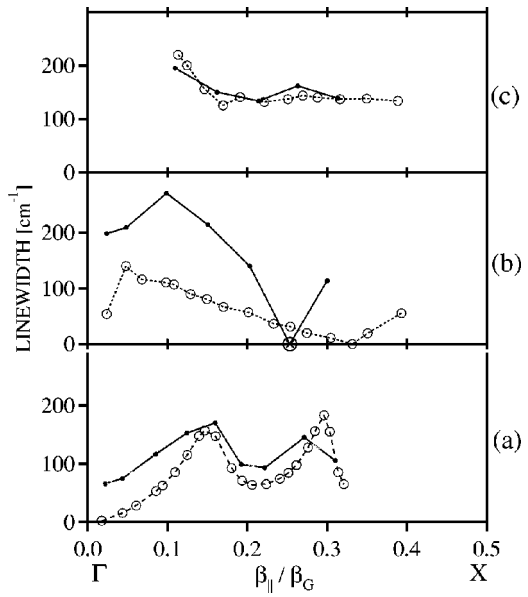

FIG. 4. Experimental (dots and solid lines) and model (open circles and dotted lines) linewidths of lowest (a), fourth lowest (b), and fifth lowest (c) band vs in-plane wave vector along the $\Gamma - X$ direction. The crossed circle represents a zero linewidth that was inferred from the absence of any feature in the spectrum.

responding modes must be made up of *pairs* of TE-polarized field components that are either in or out-of-phase with respect to each other (first order TE components lying along the line of mirror symmetry can clearly only drive *s*-oriented polarization in the zeroth order). Thus along Γ-X, going away from the second-order gap at zone center, there are 3 *s*-polarized modes. The 2 strongly dispersive modes are dominated by TE field components aligned along Γ-X, and the *s*-polarized mode with little dispersion consists primarily of a symmetric superposition of TE field components oriented nearly perpendicular to the direction of propagation. The *p*-polarized band with little dispersion consists primarily of an anti-symmetric superposition of TE field components oriented nearly perpendicular to the direction of propagation. Similar symmetry arguments immediately explain why there are two moderately dispersive pairs of modes along Γ-M, with one of each *s* and one of each *p* polarized.

Symmetry also explains the degeneracies and linewidth behavior of modes at the zone center. For a mode to have a finite lifetime (nonzero linewidth) at the zone center, it must be at least twofold degenerate because there can be no preferred polarization for the radiated field component right at normal incidence. For the same reason, modes that are nondegenerate at the zone center must have infinite lifetimes (zero linewidths) there. These symmetry properties are faithfully reproduced by our model calculations, and they are consistent with the experimentally determined lifetimes. Note that the lowest two modes essentially disappear from the spectra in Fig. 2 as they approach the zone center, while the fourth highest energy mode, which converges with the third highest energy, *p*-polarized mode at the zone center, maintains a significant linewidth.

Figure 4(a) shows the calculated and measured linewidths of the lowest-order band along the Γ-X direction. This mode is nondegenerate at zone center (see Fig. 3), and its calculated lifetime is infinite there. The finite size of the membrane, 90 μm$\times$90 μm, puts a lower limit of $\sim$60 cm^{-1} on the experimentally resolvable linewidth. However, for lifetimes greater than this lower limit, the experimental and calculated lifetimes are in good agreement, and both exhibit a strong modulation towards the zone boundary. The calculated linewidth of this mode exhibits no such modulation when the oxide cladding layer is assumed to be infinitely thick. The calculated linewidth in fact oscillates as a function of the cladding layer thicknesses. This confirms that the net strength of the radiative component of the Bloch state is strongly influenced by the vertical cavity formed by the finite thickness cladding layer. Because all of the *dominant* field components of the Bloch states in this band are evanescent in the cladding layer, and are not, therefore, influenced by the oxide layer thickness (when it exceeds $\sim$500 nm), the linewidth of the modes can be tuned over a significant range while leaving the basic mode energy essentially fixed. For these bands then, the vertical 1D oxide cavity is coupled to the 2D in-plane ''cavity,'' through the lowest-order Fourier component of the Bloch states.

Finally, we draw attention to the anticrossing between states in the two highest-energy bands along the Γ-X direction, which occurs near $\beta_\parallel / \beta_g \sim 0.25$. The energy of closest approach is comparable to the width of the gap that opens up at zone center. This implies that the corresponding modes are strongly mixed. Away from the anticrossing, towards the zone center, the modes in the fourth band are predominantly composed of a TE-polarized field component at $\beta_\parallel \hat{x} + \beta_g \hat{x}$. The modes in the fifth band below the anticrossing are predominantly composed of a symmetric superposition of TE-polarized field components at $\beta_\parallel \hat{x} - \beta_g[\hat{x} + \hat{y}]$ and $\beta_\parallel \hat{x} - \beta_g[\hat{x} - \hat{y}]$. Both have *s*-polarized radiative components and, therefore, have the appropriate relative symmetries to couple through scattering from the Fourier components of the grating at $\beta_g[\hat{x} + \hat{y}]$ and $\beta_g[\hat{x} - \hat{y}]$. Bands with opposite polarization labels do not couple, and therefore they do not anticross. States in the two bands near the anticrossing are composed primarily of three TE-polarized field components at $\beta_\parallel \hat{x} + \beta_g \hat{x}$, $\beta_\parallel \hat{x} - \beta_g[\hat{x} + \hat{y}]$ and $\beta_\parallel \hat{x} - \beta_g[\hat{x} - \hat{y}]$. The states in the fifth band consist of a symmetric superposition of all three components, while the states in the fourth band have the $\beta_\parallel \hat{x} + \beta_g \hat{x}$ component out of phase with the other two. This leads to the interesting appearance of a perfectly bound mode (zero linewidth) on the lower side of the anticrossing, away from any point of high symmetry in the lattice. The linewidths for these anti-crossing modes are shown in Figs. 4(b) and 4(c). Clearly, the calculation verifies the existence of this perfectly bound mode. The lower state disappears from the experimental reflectivity spectra in the vicinity of the anticrossing, consistent with this picture.

Note that agreement between model and experiment is somewhat poorer for both the frequency and linewidth of the fifth band. This is partly due to the fact that it lies in the vicinity of and above the electronic bandgap of GaAs, which forms roughly half of the waveguide core. In this region the model used for the dielectric constant of GaAs neglects the imaginary part and is not strictly valid even for the real part.

It is also due to the omission of higher-order Fourier components of the field, that become significant at these higher energies.

To summarize, we have fabricated a robust AlGaAs waveguide with a high-index contrast 2D photonic lattice and used resonant specular reflectivity measurements to probe the dispersion of the complex photonic band structure. The real part of the band structure exhibits a gap 10% of the center frequency that represents a substantial modification of the density of electromagnetic modes supported by the slab. The results agree extremely well with our computationally-efficient model and reveal interesting polarization symmetries of the 2D lattice. The imaginary part of the band structure, as measured by the linewidths, agrees qualitatively with the model and displays interesting features associated with coupling to the oxide cavity. Both the real and imaginary parts of the band structure exhibited anticrossing behavior suggestive of a purely bound mode away from a high-symmetry point of the square lattice at second order.

We wish to thank NSERC, the Cable Labs Fund, and the Center for Innovation in Photonics for their financial support of this work.

[1] E. Yablonovitch, Phys. Rev. Lett. **58**, 2059 (1987).
[2] S. John, Phys. Rev. Lett. **58**, 2486 (1987).
[3] K. Agi, E.R. Brown, O.B. McMahon, C. Dill III, and K.J. Malloy, Electron. Lett. **30**, (25)2166 (1994).
[4] J.D. Joannopoulos, R.D. Meade, and J.N. Winn, *Photonic Crystals* (Princeton University Press, Princeton, 1995).
[5] S. John and V.I. Rupasov, Phys. Rev. Lett. **79**, 821 (1997).
[6] T. Quang, M. Woldeyohannes, S. John, and G.S. Agarwal, Phys. Rev. Lett. **79**, 5238 (1997).
[7] M. Kanskar, P. Paddon, V. Pacradouni, R. Morin, A. Busch, J.F. Young, S.R. Johnson, J. Mackenzie, and T. Tiedje, Appl. Phys. Lett. **70**, 1438 (1997).
[8] J.D. Joannopoulos and P.R. Villeneuve *et al.*, Nature (London) **386**, 143 (1997).
[9] D.J. Ripin, K-Y Lim, G.S. Petrich, P.R. Villeneuve, S. Fan, E.R. Thoen, J.D. Joannopoulos, E.P. Ippen, and L.A. Kolodziejski, J. Appl. Phys. **87**, 1578 (2000).
[10] P. Paddon and J.F. Young, Opt. Lett. **23**, 1529 (1998).
[11] P. Paddon and J.F. Young, Phys. Rev. B **61**, 2090 (2000).
[12] A. Cowan, P. Paddon, V. Pacradouni, and J.F. Young, JOSA A (to be published).
[13] P.J. Roberts, T.A. Birks, P.St.J. Russell, T.J. Shepherd, and D.M. Atkin, Opt. Lett. **7**, 507 (1996).
[14] V.N. Astratov, D.M. Whittaker, I.S. Culshaw, R.M. Stevenson, M.S. Skolnick, T.F. Krauss, and R.M. De La Rue, Phys. Rev. B **60**, R16 255 (1999).
[15] O. Painter, R.K. Lee, A. Scherer, A. Yariv, J.D. O'Brien, P.D. Dapkus, and I. Kim, Science **284**, 1819 (1999).
[16] F. Sfigakis, P. Paddon, V. Pacradouni, M. Adamcyk, C. Nicoll, A. R. Cowan, T. Tiedje and J. F. Young, J. Lightwave Technol. **18**, 199 (2000).
[17] The parameters required by the model are the layer thicknesses, grating pitch, hole diameter, and refractive indices of the composite materials. The modelling results shown were obtained using parameter values that agreed within 3% with the nominal or measured values listed in Fig. 1. The GaAs/AlGaAs refractive indices were taken to be purely real, with dispersion and variation with alloy composition included according to Ref. 18. The oxide refractive index used was 1.6, Ref. 16.
[18] S. Adachi, Phys. Rev. B **38**, 12 345 (1988).